

Article

Climate Warming Dominates Vegetation Productivity in the Hanjiang River Basin, China

Yuhui Bao ^{1,2,3,†}, Liang Zheng ^{4,†}, Kai Zhu ^{1,2,3,†} and Hai Liu ^{1,2,3,*}

¹ Hubei Key Laboratory of Regional Development and Environmental Response, Hubei University, Wuhan 430062, China; 202121108012627@stu.hubu.edu.cn (Y.B.); zhukai@stu.hubu.edu.cn (K.Z.)

² Research Center of Territorial Space Management, Hubei University, Wuhan 430062, China

³ Faculty of Resources and Environmental Science, Hubei University, Wuhan 430062, China

⁴ State Key Laboratory of Information Engineering in Surveying, Mapping and Remote Sensing, Wuhan University, Wuhan 430079, China; liangzheng@whu.edu.cn

* Correspondence: liuhai11191@163.com

† These authors contributed equally to this work.

Abstract: The Hanjiang River Basin (HJRB) encompasses the Danjiangkou Reservoir, a critical water source for the South-to-North Water Transfer project, the world's largest such endeavor. Recent studies have highlighted that increased vegetation growth in the HJRB has led to reduced water availability in the region. To investigate the seasonal dynamics and spatial patterns of vegetation and their association with the local climate, we employed Gross Primary Productivity (GPP), a pivotal component of terrestrial carbon-water cycling, derived from the MODIS MOD17A2HGF dataset at a 500 m resolution. We combined this dataset with station meteorological data and the Standardized Precipitation Evapotranspiration Index (SPEI) to explore the complex relationship between vegetation productivity, climate fluctuations, and hydrothermal changes in the HJRB from 2000 to 2020. Our findings reveal that the rising trend in vegetation productivity in the HJRB is primarily attributable to climate warming. Different types of vegetation in the upstream and downstream areas exhibit varying water requirements. While the region has not experienced prolonged widespread drought conditions thanks to its excellent water conservation capabilities, there remains a certain level of drought risk in the downstream area as the climate continues to warm. Moreover, variables such as wind speed and sunshine duration significantly impact the hydrothermal conditions within the river basin, consequently influencing vegetation productivity. This study elucidates the mechanisms through which climate change affects vegetation productivity in the HJRB. Despite afforestation efforts in the upstream region and climate warming leading to increased greening, there may be implications for the water retention function of the HJRB. This understanding is crucial for water resource management and ecosystem sustainability in the HJRB.

Keywords: gross primary productivity; climate change; spatiotemporal characteristics



Citation: Bao, Y.; Zheng, L.; Zhu, K.; Liu, H. Climate Warming Dominates Vegetation Productivity in the Hanjiang River Basin, China. *Land* **2023**, *12*, 1891. <https://doi.org/10.3390/land12101891>

Academic Editor: Iva Apostolova

Received: 14 September 2023

Revised: 5 October 2023

Accepted: 6 October 2023

Published: 9 October 2023



Copyright: © 2023 by the authors. Licensee MDPI, Basel, Switzerland. This article is an open access article distributed under the terms and conditions of the Creative Commons Attribution (CC BY) license (<https://creativecommons.org/licenses/by/4.0/>).

1. Introduction

Vegetation plays a crucial role in Earth's ecosystems, affecting carbon and water cycles, soil conservation, biodiversity maintenance, climate regulation, air purification, and food supply [1–4]. Previous research has indicated that vegetation is influenced by various factors including climate change, water resources, natural disasters, and land use changes [5–8]. Against the backdrop of global warming, frequent extreme climate events, and rapid urbanization, monitoring vegetation dynamics and quantifying vegetation growth responses to climate change have become focal points of global and regional research, contributing significantly to understanding land vegetation ecosystem growth mechanisms and climate change adaptation [9,10].

The IPCC has pointed out the increasingly complex nature of climate change risks, with multiple disasters converging and impacting various systems simultaneously [11].

Moreover, under global warming conditions, El Niño events might become more frequent and intense, while La Niña events could become more prolonged and severe, resulting in a rise in extreme climate events [12,13]. In recent years, remote sensing technology has facilitated large-scale, long-term monitoring of land vegetation dynamics, utilizing various vegetation indices such as NDVI, EVI, LAI, and FVC to characterize surface vegetation growth [14]. Gross Primary Productivity (GPP), the total amount of photosynthetic organic matter fixed by plants in photosynthesis per unit area or volume, plays a pivotal role in ecosystem energy flow, material circulation, and carbon cycling [15]. Measuring and monitoring GPP can offer insights into solar energy utilization efficiency, changes in plant productivity, ecosystem productivity, and carbon cycling [16]. Therefore, GPP is a crucial indicator in studies related to ecosystem ecology, global carbon cycling, and climate change [17–19].

Since the 20th century, factors such as population growth, economic development, and urbanization have led to large-scale agricultural cultivation, deforestation, and environmental pollution, causing degradation and disruption of vegetation ecosystems in various regions [20–22]. However, in recent decades, numerous environmental protection and ecological restoration measures have been implemented, contributing to the recovery of degraded vegetation ecosystems [23–25]. As a result, ecological restoration projects have been widely undertaken, leading to an increase in forest area and a noticeable improvement in vegetation cover [26–28]. Nonetheless, the characteristics and dominant mechanisms of vegetation changes vary across different regions [28–31]. Previous research has highlighted temperature and precipitation as the most important climatic factors affecting vegetation growth variations [7,29,32]. Nevertheless, apart from temperature and precipitation, other climate factors also impact vegetation growth and distribution [31,33], such as solar radiation conditions influencing photosynthesis and wind speed and humidity affecting evaporation [34,35]. Although vegetation in most regions around the world is experiencing an upward trend, research has indicated that, against the backdrop of rising temperatures, water availability has become a significant limiting factor for vegetation growth [5,28]. Additionally, numerous studies have suggested that vegetation greening can influence regional water resources [36–38].

The Hanjiang River Basin (HJRB), located in central China, serves as the core water source for the Danjiangkou Reservoir, which is a crucial component of the South-to-North Water Diversion Project, the largest water diversion project in the world. Thanks to global warming and ecological engineering, the HJRB has undergone significant greening over the past few decades [39–41]. Research on the vegetation in the HJRB has indicated that precipitation and temperature are the primary climatic factors affecting NDVI changes. However, other climate factors such as wind speed, sunshine duration, and potential evapotranspiration, which directly or indirectly influence regional water and thermal conditions, and consequently impact vegetation growth and distribution, have been overlooked [35]. Recent studies have pointed out that vegetation greening has affected the availability of water resources in the HJRB [38]. Given that GPP influences water resources supply, water cycling, and water source conservation [15], it is imperative to investigate the mechanisms behind changes in vegetation productivity exacerbated by climate change. Moreover, due to the influence of monsoon climate, there are significant differences in precipitation, temperature, and various climate indicators between different seasons. Therefore, to gain an in-depth understanding of the impact of climate change on ecosystems, it is crucial to study the seasonal variations in vegetation and how vegetation productivity responds to these seasonal climate changes [42–45]. This provides essential references for devising climate change adaptation strategies and ecological conservation.

Numerous studies have delved into the relationship between vegetation and its influencing factors [7,29,46,47], with several specifically addressing vegetation dynamics in the HJRB [39–41]. However, research focusing on the seasonal characteristics of vegetation dynamics while considering multiple climate factors and drought conditions remains relatively scarce. We selected the HJRB as our study area due to its unique water conservation

function. Moreover, the pronounced differences between the upstream and downstream regions of the HJRB, characterized by diverse vegetation and vertical zones, ensure the representativeness of our study and offer insights for other similar water conservation areas. Thus, this study analyzes the spatiotemporal characteristics and response mechanisms of GPP in the HJRB from 2000 to 2020. The main objectives of this study are as follows: (1) to evaluate the seasonal vegetation productivity in the HJRB; (2) to explore the response mechanisms of GPP to climate factors; (3) to quantify the contributions of climate change to GPP variations in the HJRB. This research reveals the trends in GPP changes at the regional level on both interannual and seasonal scales, along with the response mechanisms to climate change. It holds significant importance for preserving the ecological environment of the HJRB and other similar areas.

2. Materials and Methods

2.1. Study Area

The Hanjiang River, with a total length of 1567 km, flows through the provinces of Shaanxi and Hubei in China and covers a total basin area of approximately $15.9 \times 10^4 \text{ km}^2$, making it one of the largest tributaries of the Yangtze River (Figures 1 and 2). The HJRB experiences a subtropical monsoon climate, characterized by abundant and diverse water resources. The annual precipitation varies from 700 mm to 1100 mm, with 70–80% occurring during the rainy season from May to September [38]. The upper reaches of the Hanjiang span the provinces of Qinghai, Gansu, Sichuan, and Shaanxi, featuring mountainous and hilly terrains, narrow valleys, rugged gorges, and intricate river networks. The downstream main stem flows predominantly through Hubei Province, forming a floodplain with interconnected rivers and lakes, fostering rich water resources and diverse wetland ecosystems. Furthermore, the downstream region is the core area of the Hanjiang Economic Belt, encompassing vital transportation hubs and densely populated zones, thus holding significant influence over the socio-economic development of central China.

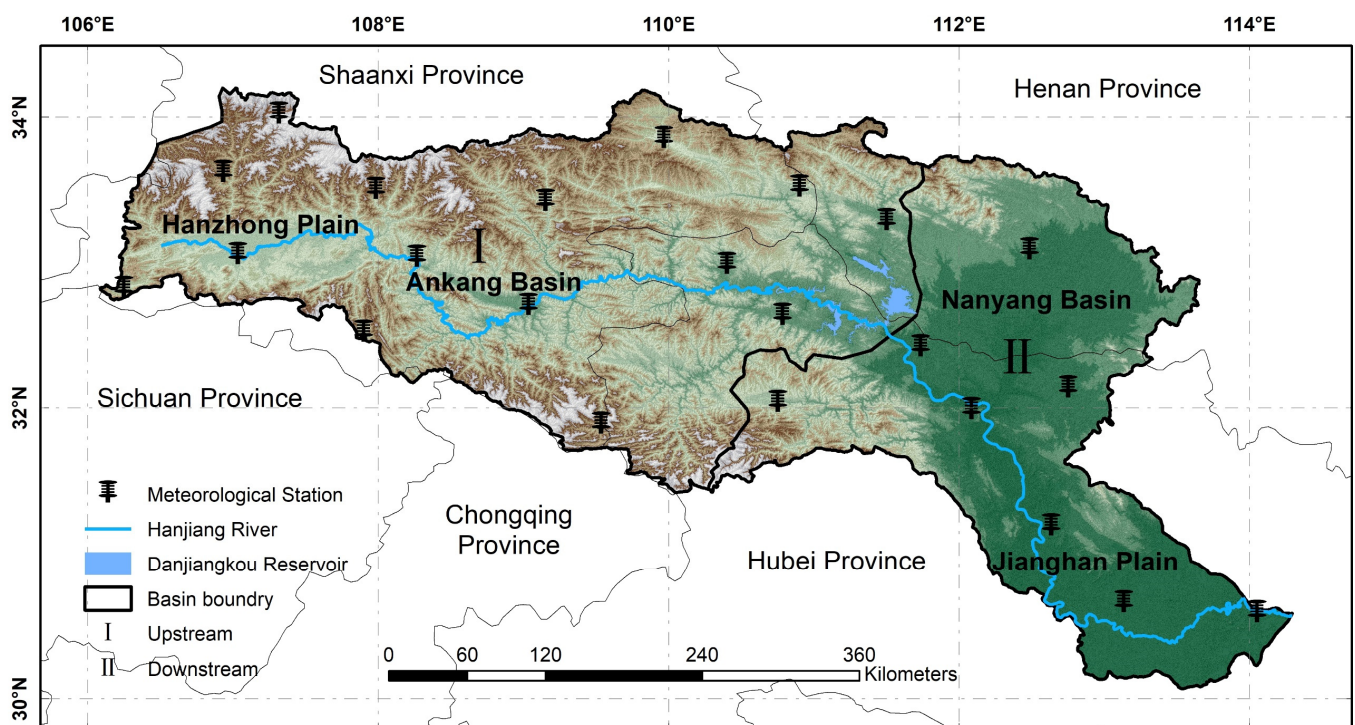


Figure 1. Location and land use of the study area.

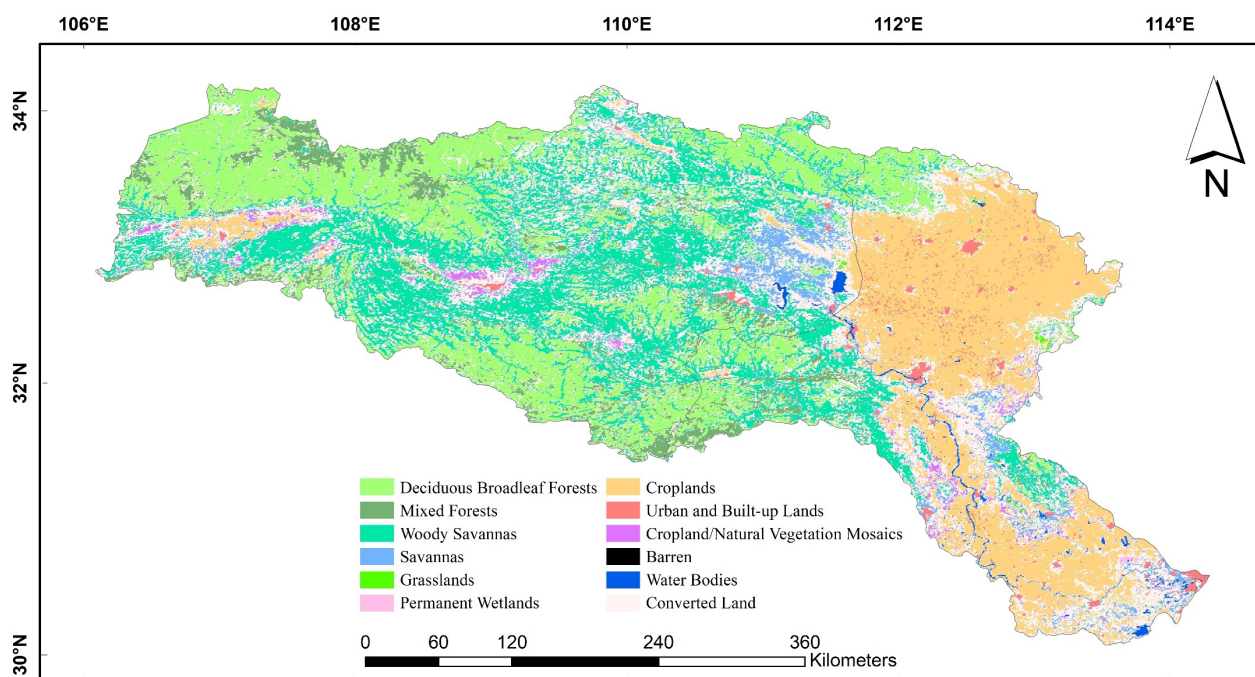


Figure 2. Distribution of LULC in the HJRB (Converted Land represents areas where changes in LULC occurred between 2001 and 2020).

2.2. Data Sources

2.2.1. GPP

The GPP data used in this study were sourced from the MODIS MOD17A2HGF version 6 product (<https://lpdaac.usgs.gov/products/mod17a2hgv006/>, accessed on 6 October 2022). This product is based on the concept of radiation use efficiency and calculates 8-day composite values of GPP. The temporal coverage spans from 2000 to 2020, with a spatial resolution of 500 m. The data underwent preprocessing steps including projection, cropping, and data format conversion to obtain monthly GPP data for the HJRB in this study.

2.2.2. Meteorological Data

The meteorological data utilized in this study were obtained from the National Meteorological Science Data Center (<http://data.cma.cn/>, accessed on 3 December 2022). The dataset includes precipitation (Pre), temperature (Tem), sunshine hours (SSD), and wind speed (WS), spanning from 2000 to 2020. Monthly values of climate factors were obtained through data aggregation and calculation. Potential evapotranspiration (PET) was computed using the Penman-Monteith method [48,49]. Furthermore, we used the Standardized Precipitation Evapotranspiration Index (SPEI), which characterizes drought at multiple scales, with SPEI1, SPEI3, and SPEI12 representing drought severity at monthly, seasonal, and annual scales in the study area, respectively. To ensure data consistency, the spatial resolution of each climate factor was interpolated to match the same spatial resolution as GPP using ANUSPLINE [50].

2.2.3. Land Use and Land Cover (LULC)

The LULC data employed in this study were derived from MODIS MCD12Q1 (<https://lpdaac.usgs.gov/products/mcd12q1v006/>, accessed on 12 October 2022). This dataset has a spatial resolution of 500 m and covers the period from 2001 to 2020. The International Geosphere-Biosphere Programme (IGBT) classification data from MCD12Q1 were utilized in this study (Figure 2 and Table 1).

Table 1. IGBP classifications along with their abbreviations (only includes LULC types in the HJRB).

Name	ID	Name	ID
Deciduous Needleleaf Forests	DNF	Grasslands	GRA
Deciduous Broadleaf Forests	DBF	Permanent Wetlands	PWL
Evergreen Broadleaf Forests	ENF	Croplands	CRO
Mixed Forests	MF	Urban and Built-up Lands	URB
Open Shrublands	OSH	Cropland/Natural Vegetation Mosaics	CVM
Woody savannas	WSA	Barren Sparse Vegetation	BSV
Savannas	SAV	Water Bodies	WAT

2.3. Methods

Figure 3 shows the processing flowchart of the data used in this study, along with the methodology employed and the workflow of the analysis results.

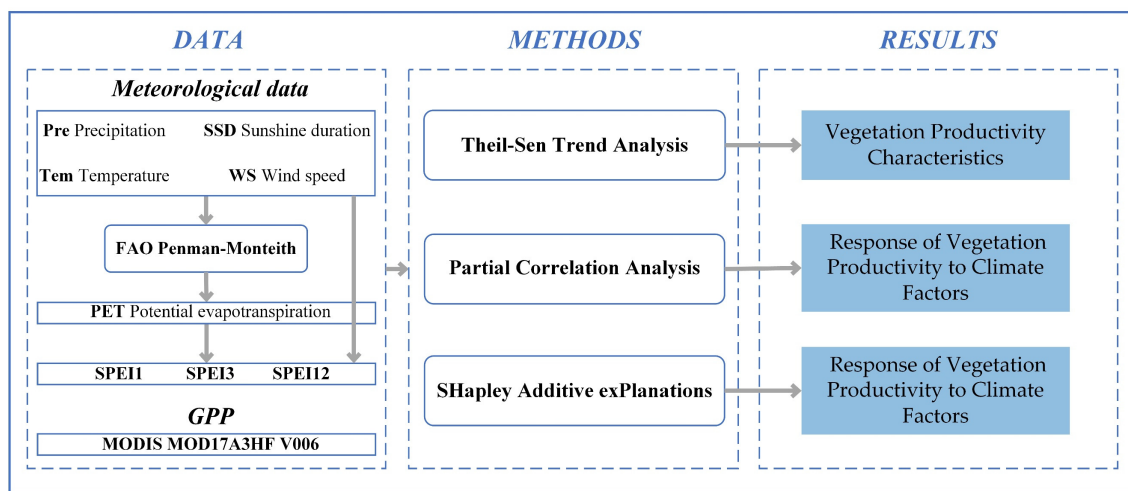


Figure 3. Data processing and analysis procedures for this study.

2.3.1. Theil-Sen Trend Analysis

The Theil-Sen trend analysis was applied pixel-wise to analyze the trend of GPP in the study area during 2000 to 2020. It is a non-parametric statistical approach that estimates the trend in an entire time series by calculating the median of the slopes between all pairs of points [51]. One advantage of this method is that it does not require the sample to follow a specific distribution and is not affected by outliers [52,53]. The formula is as follows:

$$\beta = \text{Median}\left(\frac{x_j - x_i}{j - i}\right), \forall j > i \tag{1}$$

where β represents the GPP variation trend, i and j represent the time index, x_j and x_i denote the GPP values at times i and j , respectively. The Mann-Kendall test is employed to assess the significance of trends [54].

2.3.2. Partial Correlation Analysis

We employed partial correlation analysis to elucidate the relationship between each climate variable and variations in GPP. Partial correlation analysis can eliminate the effects of covariates and focus solely on the correlation between the two variables of interest [55]. Specifically, pixel-wise partial correlation analysis was conducted to assess the response mechanism and intrinsic connections of GPP to climate variables in the HJRB from 2000 to 2020.

$$R_{xy.z} = \frac{r_{xy} - r_{xz}r_{yz}}{\sqrt{(1 - r_{xz}^2) - (1 - r_{yz}^2)}} \tag{2}$$

where $R_{xy,z}$ represents the partial correlation coefficient between x and y , z represents control variables; r_{xy} represents the correlation coefficient between x and y ; r_{xz} represents the correlation coefficient between x and z ; r_{yz} represents the correlation coefficient between y and z . The significance of partial correlation is determined through t -tests.

2.3.3. Relative Contribution Identification

We applied the SHapley Additive exPlanations approach (SHAP) to further explore the relative contribution of each climate factor. SHAP, inspired by Shapley values and based on game theory, can explain the magnitude of influence of each feature in machine learning models [56]. The SHAP approach was applied to assess the relative contribution of climate factors under different vegetation types in a linear regression model. This approach ensures equitable treatment of all features' contributions and mitigates the influence of variable order. It is commonly used for explaining various machine learning models [57,58].

3. Results

3.1. Vegetation Productivity Characteristics in the HJRB from 2000 to 2020

Figure 4a depicts the spatial distribution of GPP in the HJRB. The 21-year average of GPP shows the upstream was higher compared to the downstream, and both the southern and northern sides of the basin were higher compared to the valley within the basin. The trend of GPP in the HJRB from 2000 to 2020 is illustrated in Figure 4b, the overall distribution of GPP trends shows higher values in the valley within the HJRB, while the downstream areas exhibit a generally lower trend. Approximately 97.87% of the region demonstrates an increasing trend, with 44.62% of the area exhibiting a significant increasing trend.

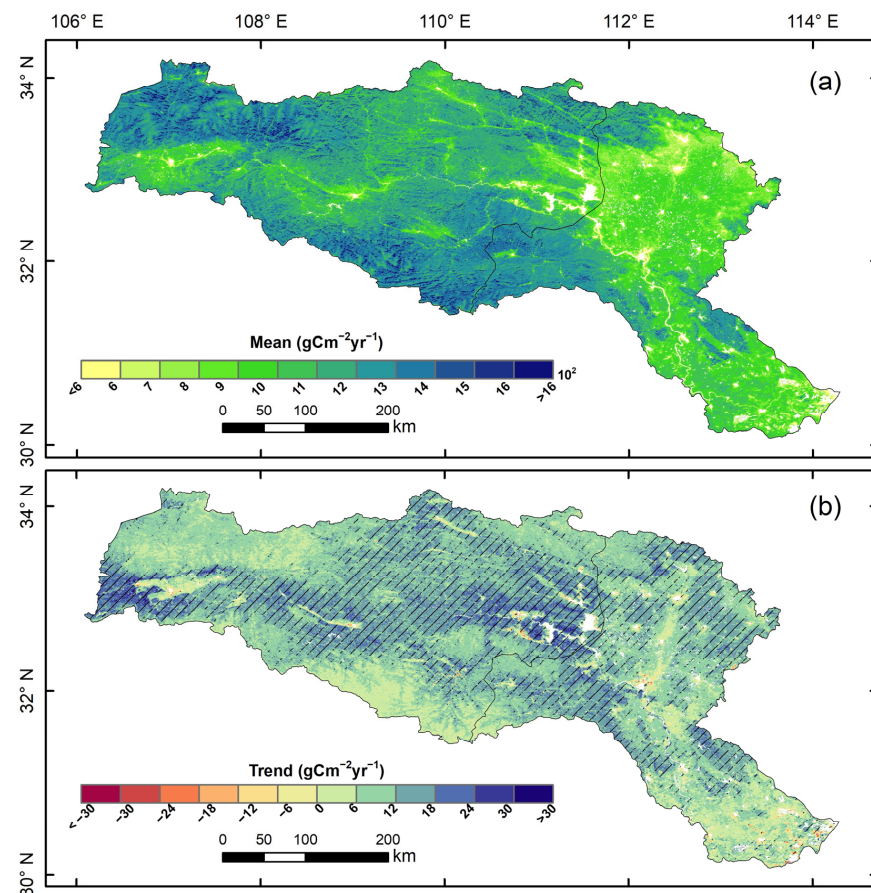


Figure 4. (a) Spatial distribution of annual average GPP in the HJRB, (b) Spatial distribution of GPP trends during 2000 to 2020 in the HJRB. Regions marked by lines indicate areas that have passed 95% significance testing.

During the period from 2000 to 2020, the average GPP in the HJRB was $1095.61 \text{ gCm}^{-2}\text{yr}^{-1}$, showing a fluctuating upward trend of $12.44 \text{ gCm}^{-2}\text{yr}^{-1}$. Figure 5 illustrates the temporal variations in GPP across various vegetation types. In the case of forests, including DBF, MF, and WSA, GPP is significantly higher compared to other vegetation types. The average GPP of DBF in the HJRB during 2000 to 2020 was $1266.97 \text{ gCm}^{-2}\text{yr}^{-1}$, higher than the other vegetation types. Grassland had the lowest mean GPP with an average of $804.97 \text{ gCm}^{-2}\text{yr}^{-1}$.

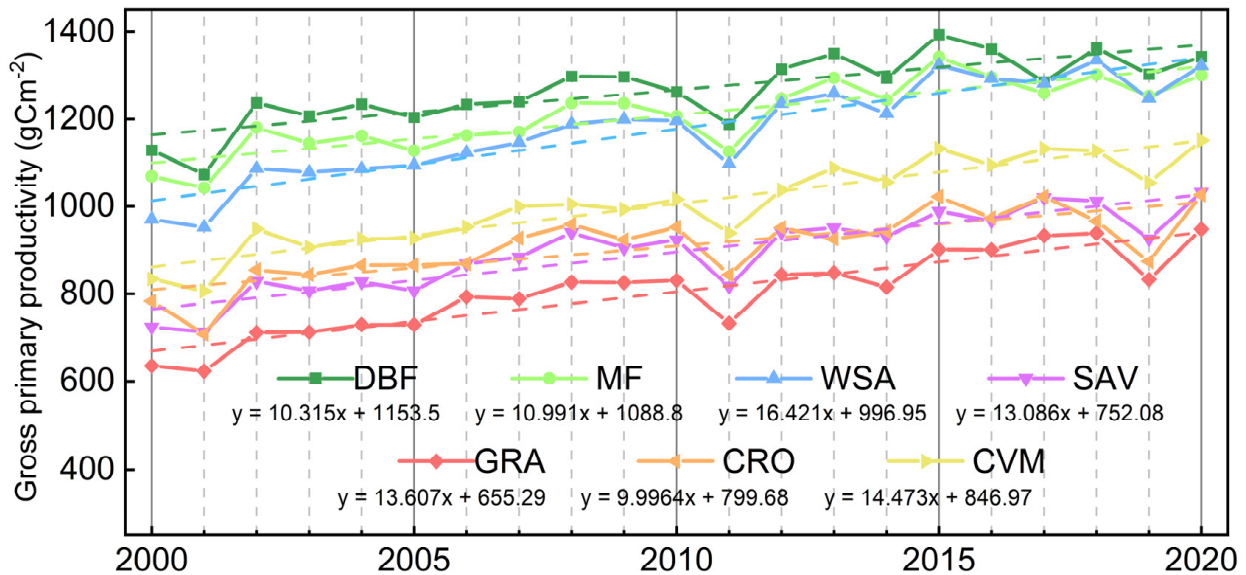


Figure 5. Interannual variation of GPP for different vegetation types in the HJRB from 2000 to 2020.

Furthermore, we conducted an analysis of multi-year averages of GPP and climate factors to investigate the seasonality of vegetation productivity in the HJRB, as illustrated in Figure 6. GPP in the HJRB attains its peak in August, with consistently higher values in the upstream region. However, from January to April, downstream GPP slightly exceeds that of the upstream. A noticeable deceleration in the growth of downstream GPP is observed from April to June, while a similar deceleration occurs in the upstream region in June. The seasonal trends of GPP generally align with those of climate factors (Tem, Pre, PET, SSD), rising in conjunction with these factors. Unlike GPP, the peak values of climate factors are recorded in July. WS displays prominent seasonality, steadily increasing from September to October, reaching its zenith in March to April of the subsequent year, and then gradually decreasing. Conversely, the SPEI drought index does not exhibit strong seasonality. In summary, the primary climatic distinction between the upstream and downstream regions in the HJRB can be attributed to temperature fluctuations associated with changes in elevation.

3.2. Response of Vegetation Productivity to Climate Factors

To investigate the impact of climate factors on vegetation productivity in the HJRB over the study period, we initially conducted partial correlation analysis to examine the relationship between multi-year averages of GPP for various vegetation types and climate factors in the HJRB (Figure 7). The findings revealed that GPP in different vegetation types within the HJRB was primarily influenced by Tem and PET. Pre exhibited a strong correlation mainly in the upstream regions, while WS and SSD showed negative correlations in both upstream and downstream areas. Drought had a relatively minor impact on GPP in the HJRB. GPP demonstrated a negative correlation with SPEI1 and a positive correlation with SPEI3 and SPEI12, with SPEI3 exerting the most significant overall influence among the SPEIs.

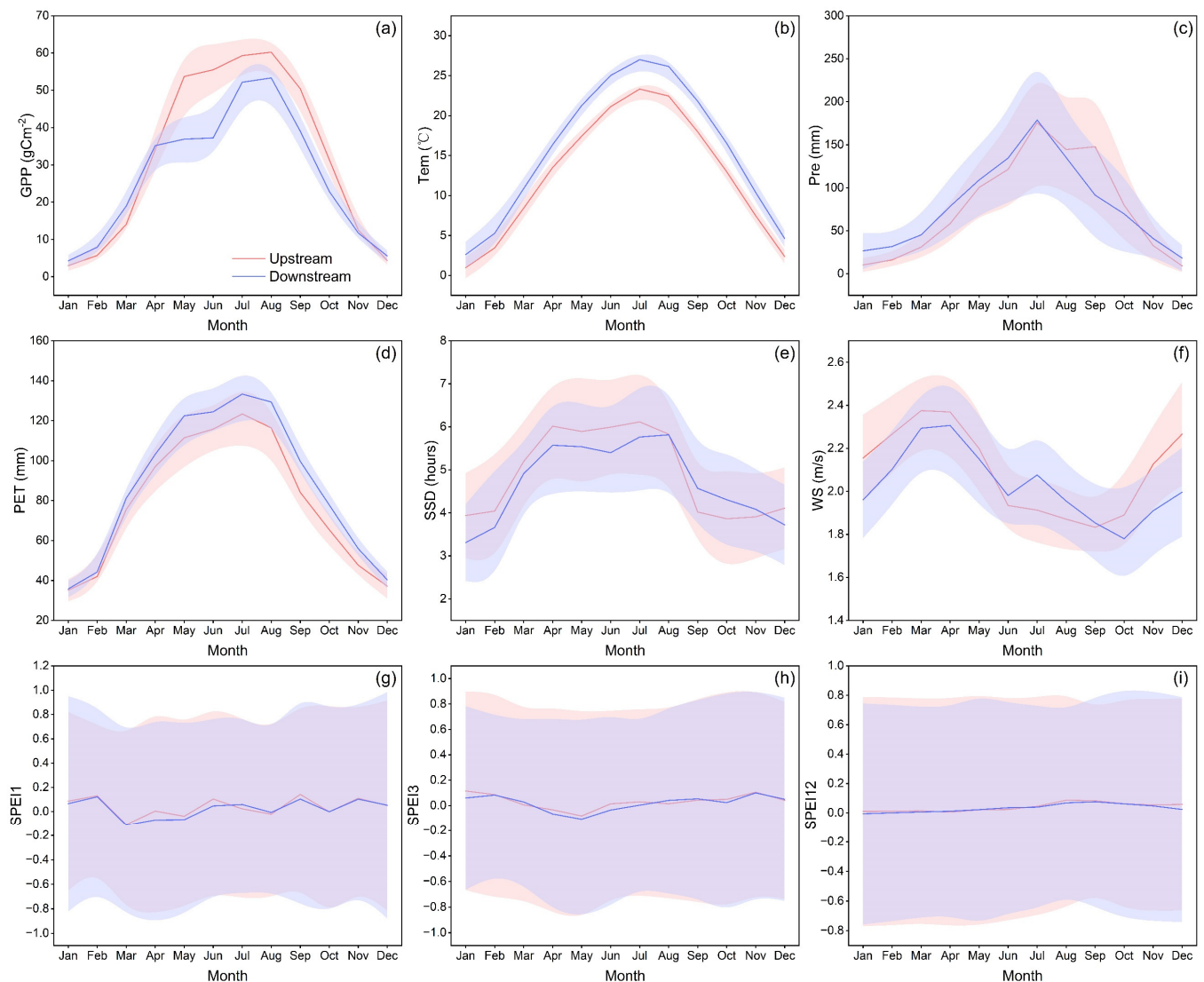


Figure 6. Seasonal variations in the multi-year average of GPP and climate factors in the HJRB: (a) GPP, (b) Tem, (c) Pre, (d) PET, (e) SSD, (f) WS, (g) SPEI1, (h) SPEI3, (i) SPEI12. Shaded areas represent standard deviations, with red and blue indicating the upstream and downstream of HJRB, respectively.

Additionally, we performed spatial partial correlation analyses between GPP and climate factors (Figure 8). Our findings reveal spatial variations in the influence of climate variables on vegetation productivity in the HJRB. Within the HJRB, 99.40% of the area displays a positive correlation with Tem, with 90.68% of this region exhibiting statistically significant positive correlations. Similarly, PET, SPEI3, and Pre demonstrate positive correlations in over 80% of the HJRB (90.34%, 94.50%, and 85.68%, respectively), with 46.42%, 56.20%, and 33.46% of these areas showing statistically significant positive correlations. In contrast, only 70.99% of the region displays a positive correlation with SPEI12, and just 7.41% of this area exhibits statistically significant positive correlations. GPP exhibits negative correlations with SPEI1, WS, and SSD in 77.44%, 69.44%, and 67.18% of the area, respectively, with statistically significant areas accounting for 9.67%, 17.18%, and 32.35%, respectively. In summary, the correlations between SSD, SPEI1, and SPEI12 with GPP are not statistically significant (significant areas <15%), while Tem, SPEI3, and PET display significant correlations (significant areas of 90.69%, 56.22%, and 44.92%, respectively). Pre and WS exhibit strong correlations only in specific regions.

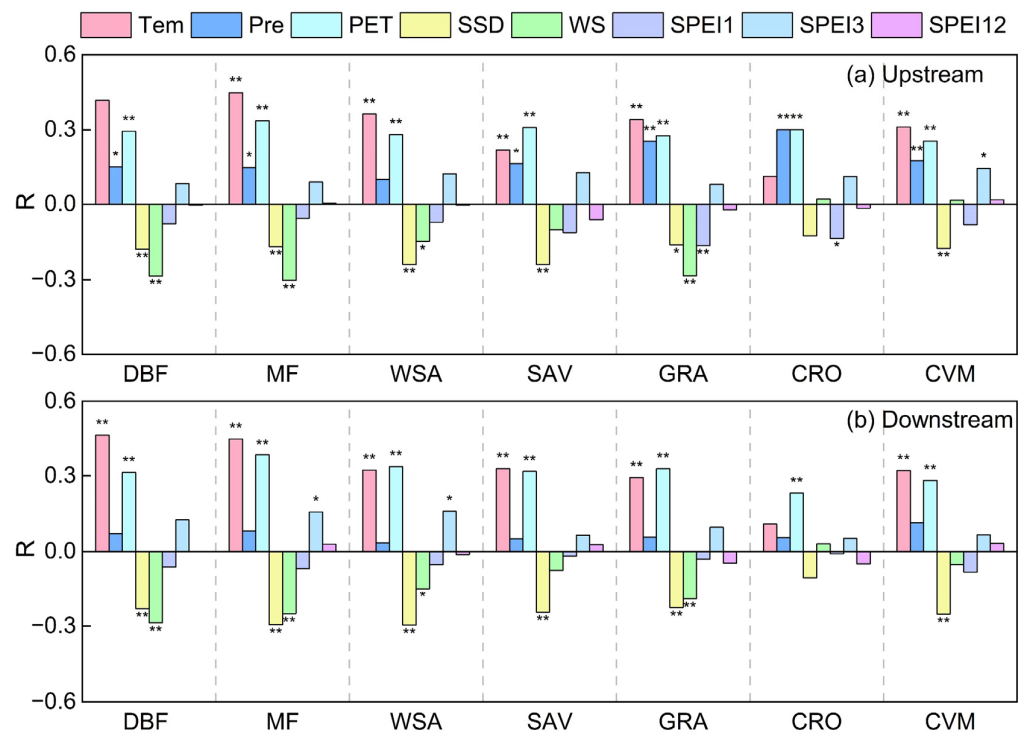


Figure 7. The partial correlations between the mean GPP of various vegetation types and climate factors for the years 2000 to 2020 for (a) the upstream and (b) the downstream regions in the HJRB. One and two asterisks (*) represent significance at the 95% and 99% levels, respectively.

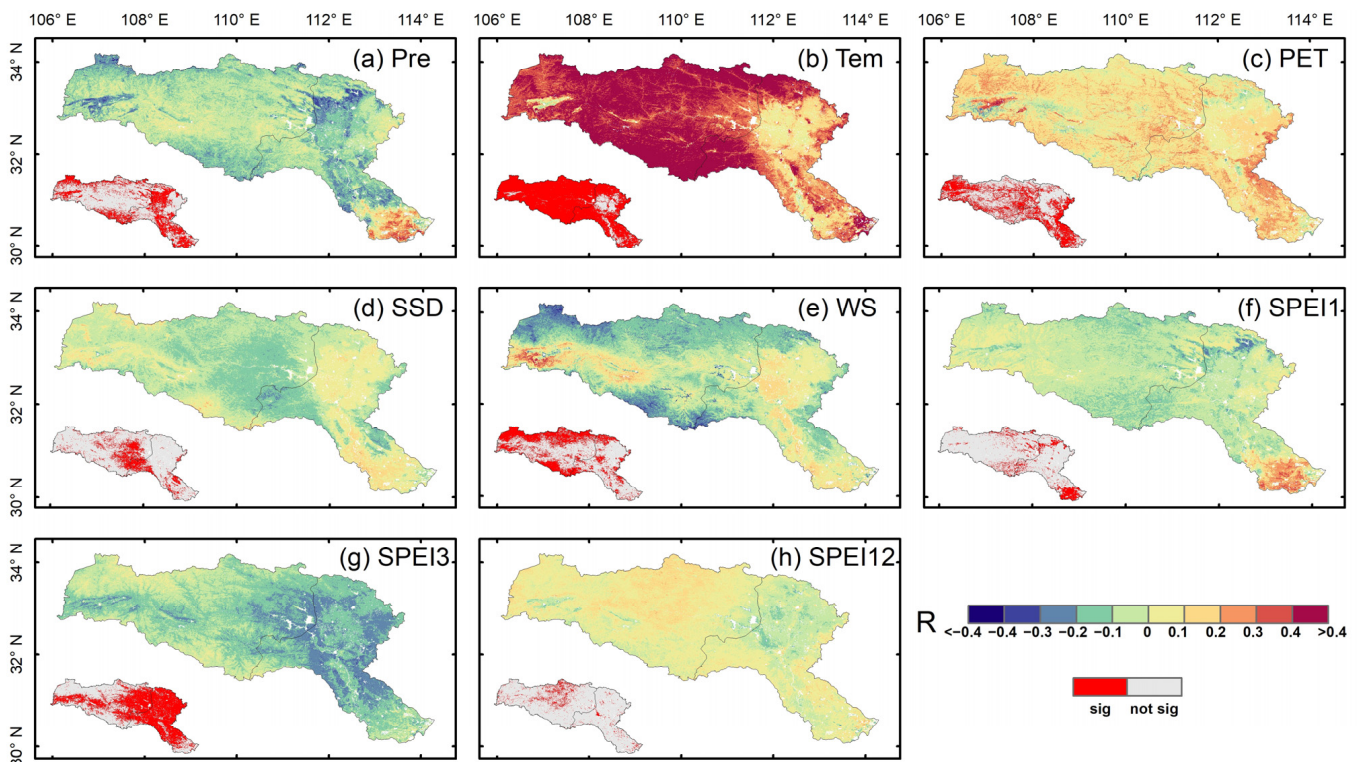


Figure 8. Spatial distribution of partial correlations between GPP and climate factors in the HJRB from 2000 to 2020.

To investigate how vegetation productivity responds to climate factors, we analyzed the temporal patterns of mean vegetation productivity in the HJRB from 2000 to 2020 in relation to changes in climate variables (Figure 9). Our study reveals distinct response patterns of GPP to various climate factors. Specifically, as Pre, Tem, PET, and WS increase, GPP gradually rises, indicating a positive influence. However, once it reaches its peak, GPP begins to exhibit a gradual decline. In contrast, SSD, initially showing a negative impact, stabilizes over time. In terms of the SPEI, we observed similar increasing effects on GPP for both SPEI3 and SPEI12. It is worth noting that GPP remains at lower levels when both SPEI3 and SPEI12 are low.

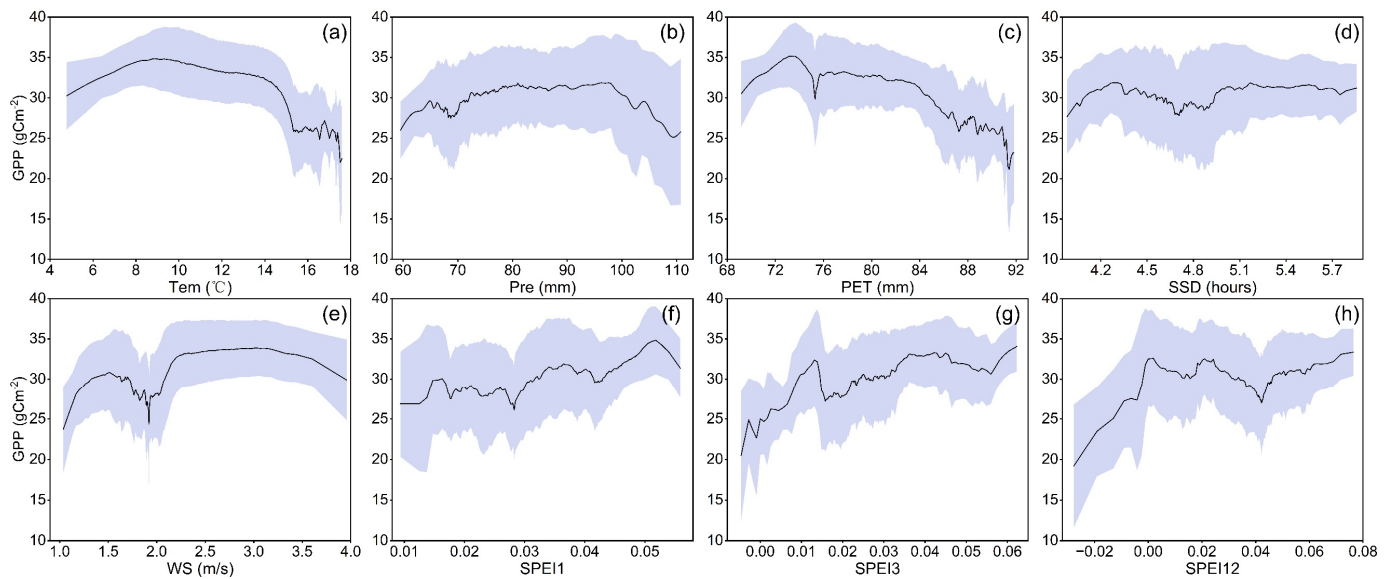


Figure 9. Response characteristics between vegetation productivity and climate factors in the HJRB from 2000 to 2020: (a) Tem, (b) Pre, (c) PET, (d) SSD, (e) WS, (f) SPEI1, (g) SPEI3, (h) SPEI12.

3.3. Contribution of Climate Factors to Vegetation Productivity

We quantified the relative contribution of each climate factor to different vegetation types in their linear models using SHAP (Figure 10). The analysis results indicate that Tem and PET have significant impacts on GPP variations in the HJRB. Consistent with the partial correlation analysis, the contribution of Pre to GPP variations is significantly higher in the upstream compared to the downstream. Tem contributes over 40% to DBF, MF, and WSA in the upstream (44.65%, 45.05%, and 42.53% respectively) and over 40% to DBF and MF in the downstream (47.23% and 40.55% respectively). PET contributes over 40% to SAV in the upstream (42.27%) and to SAV, GRA, and CRO in the downstream (43.67%, 40.74%, and 56.30%, respectively), while it is close to 40% in WSA and CVM (39.99% and 38.57%, respectively). Notably, Pre only contributes over 10% in GRA in the upstream (11.86%). The contribution of SPEIs is limited in all vegetation types. Comparatively, SPEI1 and SPEI3 have higher contribution rates than SPEI12, indicating that vegetation productivity in the HJRB is more sensitive to short-term drought conditions. The contribution rates of SSD and WS show minor differences between upstream and downstream. WS contributes significantly (>5%) in forest (DBF and MF) and just over 5% in GRA among other vegetation types. SSD contributes between 5 and 10% in all vegetation types with minimal differences.

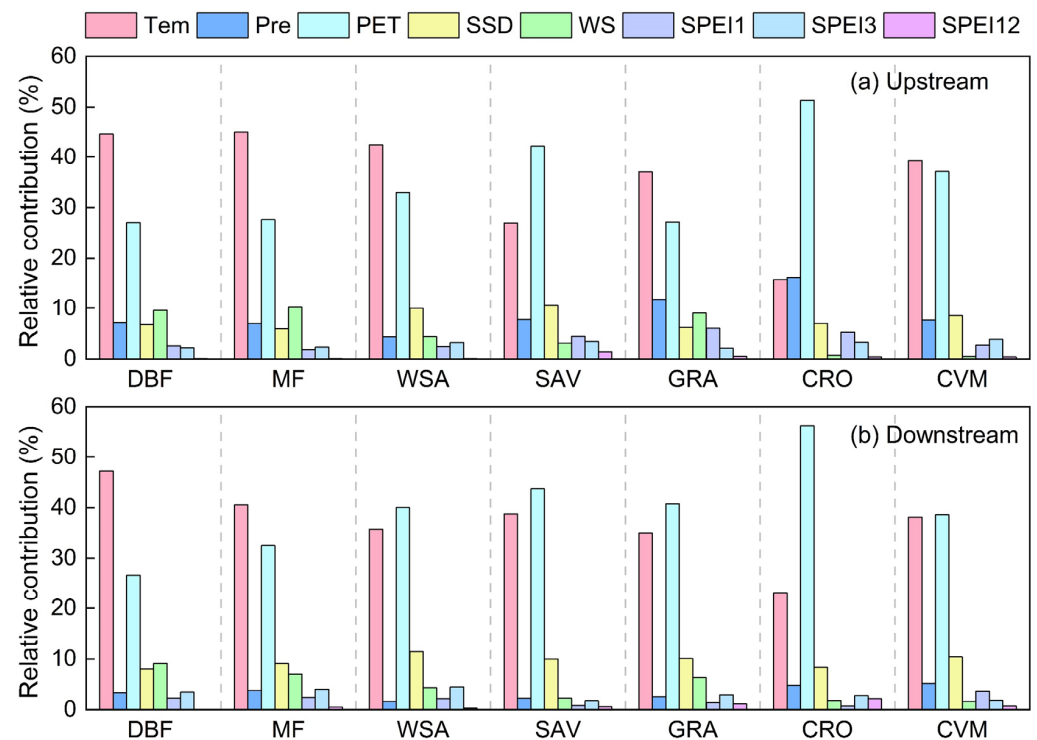


Figure 10. Relative contributions of climate factors to vegetation productivity in the HJRB from 2000 to 2020.

4. Discussion

4.1. Seasonal Pattern of Vegetation Productivity in the HJRB

From 2000 to 2020, the GPP in the HJRB displayed a significant increase, consistent with previous research on NDVI in the same region [39–41]. The spatial distribution of GPP in the HJRB revealed higher values upstream than downstream, with elevated values in the northern and southern regions compared to the valley. However, the patterns of GPP growth did not follow the same distribution; significant growth areas were concentrated near the valley, the middle reaches close to the Danjiangkou Reservoir, and in the downstream mountainous regions, including certain farmland areas. Located in a subtropical monsoon region with average annual temperatures above 0 °C, the HJRB experiences pronounced annual temperature fluctuations. Precipitation concentrates between June and September, resulting in distinct seasonal variations. The seasonal trend of GPP primarily depends on climate factors such as temperature, precipitation, PET, and SSD. In contrast to climate factors, GPP reaches its peak in August, while most climate factors peak in July, indicating a lag in the response of GPP to climate factors. Furthermore, a slowdown in the growth trends of GPP is observed in both the upstream and downstream regions of the HJRB in June and from April to June. This slowdown is mainly attributed to winter cultivation practices in the upstream Hanzhong Plain, HJRB Valley, and downstream Jiangnan Plain and Nanyang Basin, where winter crops like rice and wheat are harvested. The downstream area, characterized by extensive cropland, exhibits more significant and prolonged slowdown trends compared to the upstream. Despite significant variations in seasonal precipitation within the HJRB, the overall seasonal drought conditions remain relatively stable. As the temporal scale increases, the seasonal variation of the SPEI index in the HJRB becomes more stable, with the average SPEI12 remaining steady around 0 throughout the year. This indicates that despite the evident temperature rise over the past 21 years, the long-term hydrometeorological conditions in the HJRB have remained relatively stable. SPEI1 and SPEI3 are lower in February to May compared to other months, suggesting a lack of spring precipitation that affects vegetation growth.

4.2. Response Mechanisms of Vegetation Productivity to Climate Change in the HJRB

In the context of global warming, the HJRB also experienced a warming trend, particularly in the central part of the basin (Figure 11). Despite this warming trend, there was no significant increase in Pre in the HJRB. In fact, the northeastern part of the downstream basin, specifically the Nanyang Basin, experienced a significant decrease in Pre, exacerbating the region's aridity. As a result, the increased Tem and SSD led to a significant increase in PET near the Nanyang Basin. However, despite the gradual growth of GPP in the downstream Nanyang Basin, it still exhibited a significant upward trend. We hypothesize that this is mainly attributable to the continuous enhancement in agricultural productivity in the downstream over the past centuries, along with extensive irrigation in the region, which compensated for the regional aridity. Consequently, a significant negative correlation was observed between Pre and GPP in the Nanyang Basin (Figure 8). Regarding the impact of drought on GPP in the HJRB, a previous study indicated that the basin experienced relatively severe droughts in 2001–2002, 2006–2008, and 2012–2014. During our study period (2000–2020), reduced GPP was observed in 2001, 2011, 2014, 2017, and 2019 (Figure 5), suggesting that drought primarily influenced short to medium-term GPP variations in the HJRB. In the long term, the water conservation functions of the upstream forests and the Danjiangkou Reservoir in the middle reaches ensured a stable water supply for the HJRB. Furthermore, the study observed that despite significant differences in seasonal precipitation within the HJRB, the seasonal drought conditions remained relatively stable. As the temporal scale increased, the seasonal variation of the SPEI in the HJRB became more stable, with SPEI12 remaining around 0 throughout the year (Figure 6). This indicates that despite the evident temperature rise in the study period, the regional long-term hydrometeorological conditions in the HJRB have remained relatively stable. SPEI1 and SPEI3 were lower from February to May compared to other months, suggesting a lack of spring precipitation affecting vegetation growth. Additionally, the study indicated that the mISDI in the downstream and upstream valleys of the HJRB exhibited a significant downward trend [59]. This aligns with our trend analysis of SPEIs, illustrating that, in the context of continuous warming temperatures, there is a significant drought risk in the downstream HJRB, particularly during the relatively dry spring season. This also explains why croplands in the upstream HJRB have a significant correlation with precipitation, while in the downstream, the correlation is not significant, indicating that downstream croplands rely more on irrigation than precipitation.

Among the various climate factors, WS and SSD significantly influence variations in GPP in the HJRB. A study focusing on the global vegetation response to WS variations suggests that decreased WS in water-limited areas can reduce vegetation transpiration rates, thus limiting vegetation growth [60]. Conversely, in wind-resistant forest areas, increased WS can enhance material exchange and promote vegetation growth. Similar patterns were observed in the HJRB. In the mid-high altitude forest areas of the basin, the decline in WS reduced regional vegetation transpiration rates, impacting material exchange in these areas. Furthermore, a trend of increasing WS from October to the following March was observed in the HJRB, while WS continued to decrease during the summer when vegetation activity is at its peak. This undoubtedly affected regional vegetation material exchange, resulting in a significant overall negative correlation primarily observed in forested areas. The region's SSD experienced a considerable decrease, which would impact solar radiation and consequently affect vegetation photosynthesis. Typically, a positive correlation is expected when assessing the impact of SSD and Pre on vegetation [31,33]. However, within the HJRB, a widespread negative correlation has been observed. We speculate that this is primarily due to significant reductions in SSD and Pre in specific regions of the HJRB, despite an overall substantial increase in GPP. Additionally, vegetation response to climate factors may have a certain lag [33,46,47], and neglecting this lag may result in some bias.

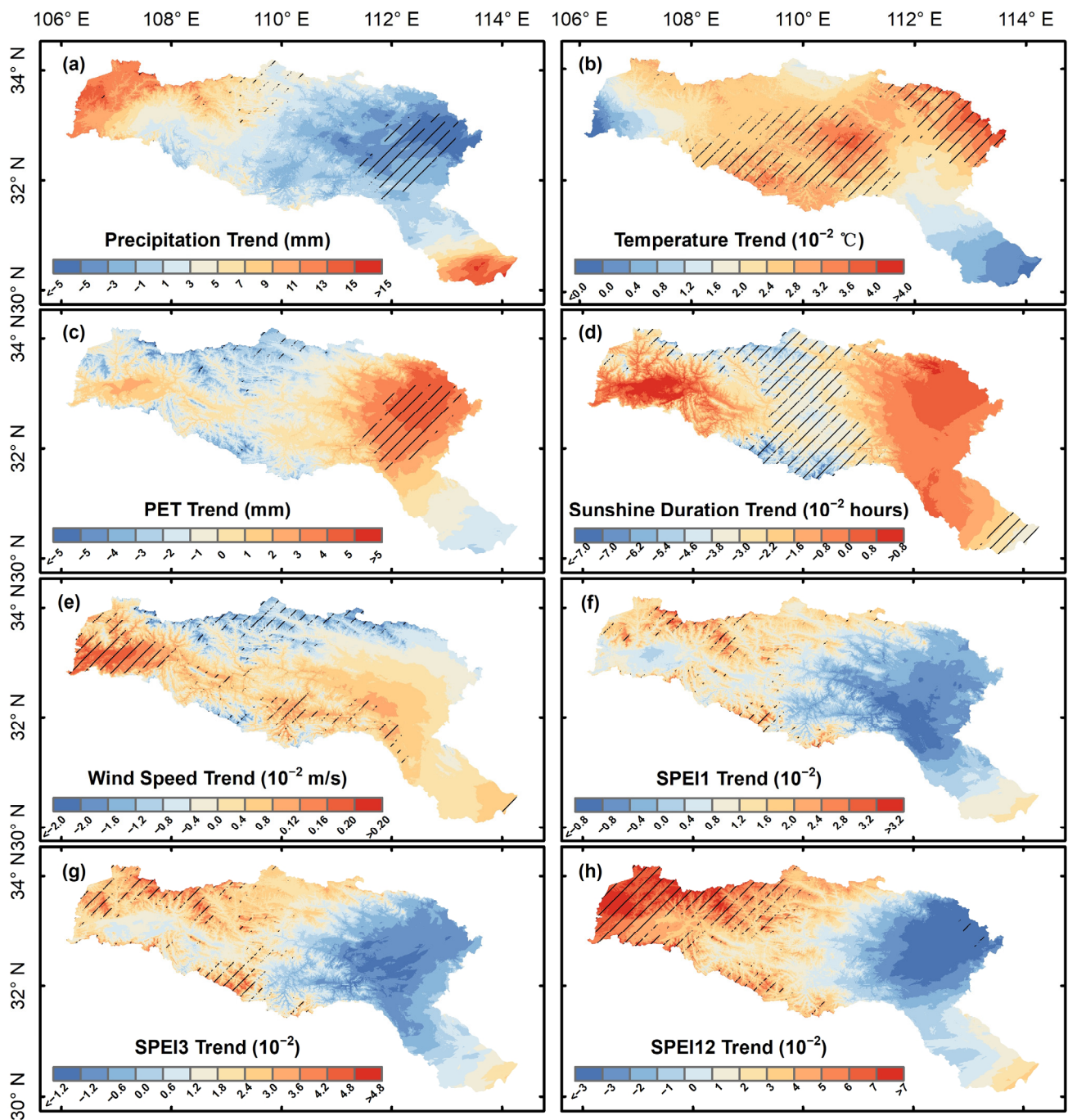


Figure 11. Spatial variation trend of climate factors in the HJRB from 2000 to 2020: (a) Pre, (b) Tem, (c) PET, (d) SSD, (e) WS, (f) SPEI1, (g) SPEI3, (h) SPEI12. Regions marked by lines indicate areas that have passed 95% significance testing.

After quantifying the contributions of climate factors to GPP changes using SHAP, we found that the contributions of Tem and PET were significantly higher than those of other climate factors. Moreover, PET dominated vegetation land cover types with weaker water storage capacity, such as CRO and SAV, while Tem played a predominant role in land cover types with stronger water storage capacity, such as DBF and MF. The warming trend undoubtedly led to an increase in PET in the HJRB. However, actual evapotranspiration depends on regional water availability. We speculate that in these land cover types where vegetation has a high demand for water but weak water storage capacity, they can obtain sufficient water supply under the premise of overall warming. This

phenomenon is more pronounced in agricultural fields relying on artificial irrigation and also affects the mid-high altitude forests relying mainly on natural precipitation. Therefore, although climate warming governs vegetation productivity changes in the HJRB, it is simultaneously constrained by regional water availability [5].

4.3. Land Use Change Patterns in the HJRB

We conducted an analysis of the land use changes in the HJRB over the past 20 years (Figure 12). The results revealed a 19.52% increase in DBF in the HJRB from 2001 to 2010, and a subsequent 6.01% increase from 2010 to 2020. This growth can be primarily attributed to large-scale afforestation efforts in the upper reaches of the HJRB, leading to a notable increase in forest density. In particular, the conversion of WSA to DBF resulted in a significant enhancement of GPP in specific upper reaches [39]. Additionally, the cultivated land in the HJRB demonstrated a shift from an increase to a decrease. The area of cultivated land expanded by a total of 5.86% between 2001 and 2010, but saw a decrease of 6.84% in the following decade. This decrease was mainly concentrated in the forest-agriculture transitional zones in the middle and upper reaches of the basin. Consistent with urbanization trends, urban land in the HJRB continuously expanded over the past two decades, marking a 17.49% increase between 2001 and 2020. These areas are primarily located around established urban zones, contributing to significant GPP degradation around major urban clusters in the basin. This aligns with previous research findings [39,41].

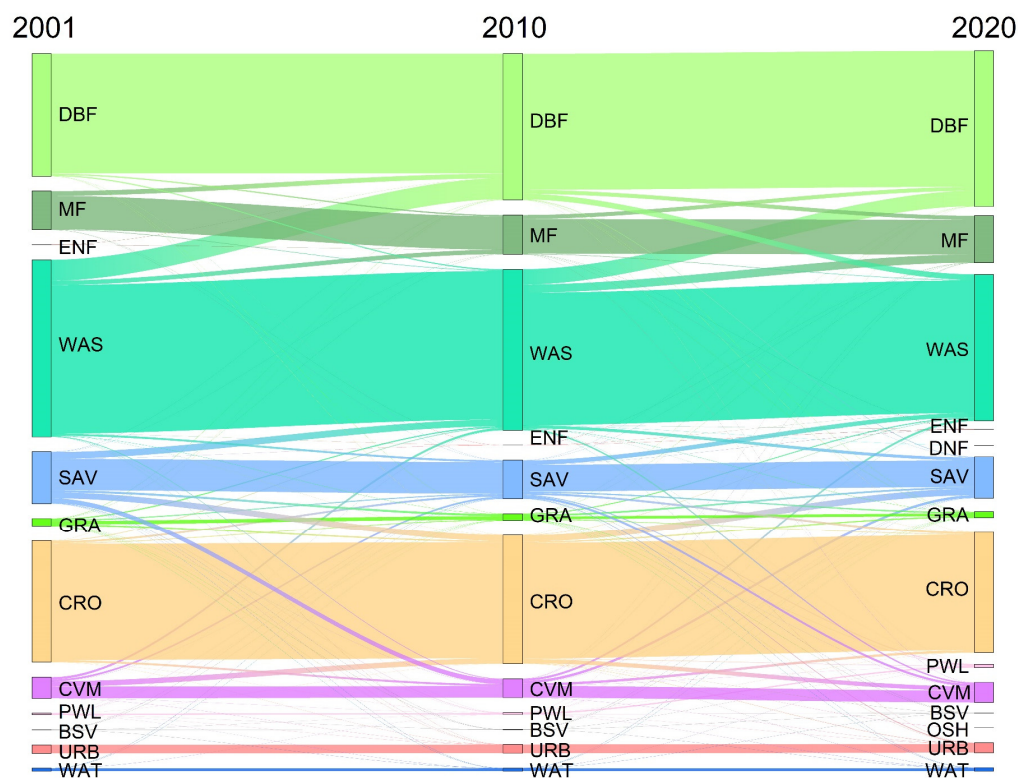


Figure 12. Sankey diagram of LULC changes in the HJRB.

4.4. Limitations

The impact of climate on vegetation productivity is highly complex, involving lag effects of climate factors, extreme climate events, regional changes in water resources, and carbon dioxide concentration. All of these factors exert direct or indirect influences on vegetation growth processes [6,61–63]. In addition, human activities also contribute to vegetation dynamics through various factors, such as population and livestock increases, urban expansion, afforestation, and reforestation [7,64]. Therefore, it is necessary to fur-

ther investigate the dynamic changes of GPP and its influencing factors. Although the SHAP analysis was applied to a multivariate linear model, an increasing body of research highlights the strong nonlinear characteristics in vegetation and climate changes. Thus, linear-based estimations inevitably run the risk of overestimating or underestimating the significance of factors. The application of nonlinear models can better capture the relationship between vegetation and climate changes. Furthermore, an accumulating effect of climate is increasingly recognized as a pivotal factor in the influence of climate on vegetation [6,46,65,66]. Consequently, future studies should comprehensively consider other environmental factors that impact vegetation dynamics, deeply explore the physiological and phenological features of GPP in the HJRB, and establish physical models to describe the processes by which driving factors affect it.

5. Conclusions

In this study, we investigated the response mechanisms of vegetation productivity to climate change in the HJRB using GPP data and meteorological station datasets, including SPEI, spanning from 2000 to 2020. The vegetation productivity in HJRB exhibited obvious spatial heterogeneity, with pronounced vegetation activity concentrated in the upstream region. Over the past 21 years, most areas of the HJRB have shown an increasing trend in vegetation productivity, with the highest increases observed in the middle reaches. Vegetation productivity was primarily influenced by *Tem*, while the water use in the upper and lower reaches was dominated by precipitation and irrigation, respectively. Additionally, the varying contributions of PET in different vegetation types revealed distinct water requirements. Furthermore, land use changes in the HJRB reflected trends such as afforestation, reforestation, and urban expansion. This study highlights that water availability to some extent influences the greening trend of vegetation in the HJRB. Despite the abundant water resources in the HJRB, there remains a certain level of drought risk in the context of ongoing warming. Future research employing more refined carbon-water coupling models can quantitatively assess the relationship between water yield and vegetation greening in the context of climate warming, providing valuable guidance for water resource conservation and ecosystem management in the HJRB region.

Author Contributions: Conceptualization, Y.B. and L.Z.; methodology, Y.B.; validation, Y.B., L.Z. and K.Z.; formal analysis, Y.B.; investigation, Y.B.; data curation, Y.B.; writing—original draft preparation, Y.B.; writing—review and editing, H.L., L.Z. and K.Z.; visualization, Y.B.; supervision, H.L.; project administration, H.L.; funding acquisition, H.L. All authors have read and agreed to the published version of the manuscript.

Funding: This research was funded by the National Natural Science Foundation of China (Project No. 42271318 No. 41971402).

Data Availability Statement: The data presented in this study are available on reasonable request from the corresponding author.

Conflicts of Interest: The authors declare no conflict of interest.

References

1. Simonich, S.L.; Hites, R.A. Importance of Vegetation in Removing Polycyclic Aromatic Hydrocarbons from the Atmosphere. *Nature* **1994**, *370*, 49–51. [[CrossRef](#)]
2. Zhou, P.; Luukkanen, O.; Tokola, T.; Nieminen, J. Effect of Vegetation Cover on Soil Erosion in a Mountainous Watershed. *Catena* **2008**, *75*, 319–325. [[CrossRef](#)]
3. Thom, D.; Rammer, W.; Seidl, R. The Impact of Future Forest Dynamics on Climate: Interactive Effects of Changing Vegetation and Disturbance Regimes. *Ecol. Monogr.* **2017**, *87*, 665–684. [[CrossRef](#)]
4. Konings, A.G.; Saatchi, S.S.; Frankenberg, C.; Keller, M.; Leshyk, V.; Anderegg, W.R.L.; Humphrey, V.; Matheny, A.M.; Trugman, A.; Sack, L.; et al. Detecting Forest Response to Droughts with Global Observations of Vegetation Water Content. *Glob. Change Biol.* **2021**, *27*, 6005–6024. [[CrossRef](#)]
5. Jiao, W.; Wang, L.; Smith, W.K.; Chang, Q.; Wang, H.; D’Odorico, P. Observed Increasing Water Constraint on Vegetation Growth over the Last Three Decades. *Nat. Commun.* **2021**, *12*, 3777. [[CrossRef](#)] [[PubMed](#)]

6. Ding, Y.; Li, Z.; Peng, S. Global Analysis of Time-Lag and -Accumulation Effects of Climate on Vegetation Growth. *Int. J. Appl. Earth Obs. Geoinf.* **2020**, *92*, 102179. [[CrossRef](#)]
7. Wei, Y.; Lu, H.; Wang, J.; Wang, X.; Sun, J. Dual Influence of Climate Change and Anthropogenic Activities on the Spatiotemporal Vegetation Dynamics Over the Qinghai-Tibetan Plateau From 1981 to 2015. *Earth's Future* **2022**, *10*, e2021EF002566. [[CrossRef](#)]
8. Wellmann, T.; Schug, F.; Haase, D.; Pflugmacher, D.; Van Der Linden, S. Green Growth? On the Relation between Population Density, Land Use and Vegetation Cover Fractions in a City Using a 30-Years Landsat Time Series. *Landsc. Urban Plan.* **2020**, *202*, 103857. [[CrossRef](#)]
9. Diener, A.; Mudu, P. How Can Vegetation Protect Us from Air Pollution? A Critical Review on Green Spaces' Mitigation Abilities for Air-Borne Particles from a Public Health Perspective—with Implications for Urban Planning. *Sci. Total Environ.* **2021**, *796*, 148605. [[CrossRef](#)]
10. Verrall, B.; Pickering, C.M. Alpine Vegetation in the Context of Climate Change: A Global Review of Past Research and Future Directions. *Sci. Total Environ.* **2020**, *748*, 141344. [[CrossRef](#)]
11. Zhongming, Z.; Linong, L.; Xiaona, Y.; Wangqiang, Z.; Wei, L. *AR6 Synthesis Report: Climate Change 2022; The Intergovernmental Panel on Climate Change (IPCC): Geneva, Switzerland, 2022.*
12. Collins, M.; An, S.-I.; Cai, W.; Ganachaud, A.; Guilyardi, E.; Jin, F.-F.; Jochum, M.; Lengaigne, M.; Power, S.; Timmermann, A.; et al. The Impact of Global Warming on the Tropical Pacific Ocean and El Niño. *Nat. Geosci.* **2010**, *3*, 391–397. [[CrossRef](#)]
13. Geng, T.; Jia, F.; Cai, W.; Wu, L.; Gan, B.; Jing, Z.; Li, S.; McPhaden, M.J. Increased Occurrences of Consecutive La Niña Events under Global Warming. *Nature* **2023**, *619*, 774–781. [[CrossRef](#)] [[PubMed](#)]
14. Bannari, A.; Morin, D.; Bonn, F.; Huete, A.R. A Review of Vegetation Indices. *Remote Sens. Rev.* **1995**, *13*, 95–120. [[CrossRef](#)]
15. Anav, A.; Friedlingstein, P.; Beer, C.; Ciais, P.; Harper, A.; Jones, C.; Murray-Tortarolo, G.; Papale, D.; Parazoo, N.C.; Peylin, P.; et al. Spatiotemporal Patterns of Terrestrial Gross Primary Production: A Review: GPP Spatiotemporal Patterns. *Rev. Geophys.* **2015**, *53*, 785–818. [[CrossRef](#)]
16. Roy, J.; Mooney, H.A.; Saugier, B. *Terrestrial Global Productivity*; Elsevier: Amsterdam, The Netherlands, 2001; ISBN 0-08-051872-9.
17. Bai, Y.; Li, S.; Liu, M.; Guo, Q. Assessment of Vegetation Change on the Mongolian Plateau over Three Decades Using Different Remote Sensing Products. *J. Environ. Manag.* **2022**, *317*, 115509. [[CrossRef](#)] [[PubMed](#)]
18. Feng, X.; Fu, B.; Zhang, Y.; Pan, N.; Zeng, Z.; Tian, H.; Lyu, Y.; Chen, Y.; Ciais, P.; Wang, Y.; et al. Recent Leveling off of Vegetation Greenness and Primary Production Reveals the Increasing Soil Water Limitations on the Greening Earth. *Sci. Bull.* **2021**, *66*, 1462–1471. [[CrossRef](#)]
19. Zhang, Z.; Ju, W.; Zhou, Y.; Li, X. Revisiting the Cumulative Effects of Drought on Global Gross Primary Productivity Based on New Long-term Series Data (1982–2018). *Glob. Change Biol.* **2022**, *28*, 3620–3635. [[CrossRef](#)]
20. Zhang, Y.; Ding, J.; Wang, Y.; Zhang, Y.; Liu, Y.; Zhang, L.; Ariken, M.; Wulan, T.; Huang, W.; Li, Y.; et al. Reconstruction of Human-Induced Forest Loss in China during 1900–2000. *Remote Sens.* **2023**, *15*, 3831. [[CrossRef](#)]
21. Sand-Jensen, K.; Pedersen, N.L.; Thorsgaard, I.; Moeslund, B.; Borum, J.; Brodersen, K.P. 100 Years of Vegetation Decline and Recovery in Lake Fure, Denmark. *J. Ecol.* **2008**, *96*, 260–271. [[CrossRef](#)]
22. Motzkin, G.; Foster, D.; Allen, A.; Harrod, J.; Boone, R. Controlling Site to Evaluate History: Vegetation Patterns of a New England Sand Plain. *Ecol. Monogr.* **1996**, *66*, 345–365. [[CrossRef](#)]
23. Chen, Y.; Feng, X.; Tian, H.; Wu, X.; Gao, Z.; Feng, Y.; Piao, S.; Lv, N.; Pan, N.; Fu, B. Accelerated Increase in Vegetation Carbon Sequestration in China after 2010: A Turning Point Resulting from Climate and Human Interaction. *Glob Change Biol* **2021**, *27*, 5848–5864. [[CrossRef](#)]
24. Li, S.; Liang, W.; Fu, B.; Lü, Y.; Fu, S.; Wang, S.; Su, H. Vegetation Changes in Recent Large-Scale Ecological Restoration Projects and Subsequent Impact on Water Resources in China's Loess Plateau. *Sci. Total Environ.* **2016**, *569–570*, 1032–1039. [[CrossRef](#)]
25. González, E.; Sher, A.A.; Tabacchi, E.; Masip, A.; Poulin, M. Restoration of Riparian Vegetation: A Global Review of Implementation and Evaluation Approaches in the International, Peer-Reviewed Literature. *J. Environ. Manag.* **2015**, *158*, 85–94. [[CrossRef](#)]
26. Chen, C.; Park, T.; Wang, X.; Piao, S.; Xu, B.; Chaturvedi, R.K.; Fuchs, R.; Brovkin, V.; Ciais, P.; Fensholt, R.; et al. China and India Lead in Greening of the World through Land-Use Management. *Nat. Sustain.* **2019**, *2*, 122–129. [[CrossRef](#)]
27. Song, W.; Feng, Y.; Wang, Z. Ecological Restoration Programs Dominate Vegetation Greening in China. *Sci. Total Environ.* **2022**, *848*, 157729. [[CrossRef](#)]
28. Piao, S.; Wang, X.; Park, T.; Chen, C.; Lian, X.; He, Y.; Bjerke, J.W.; Chen, A.; Ciais, P.; Tømmervik, H.; et al. Characteristics, Drivers and Feedbacks of Global Greening. *Nat. Rev. Earth Environ.* **2019**, *1*, 14–27. [[CrossRef](#)]
29. Gao, W.; Zheng, C.; Liu, X.; Lu, Y.; Chen, Y.; Wei, Y.; Ma, Y. NDVI-Based Vegetation Dynamics and Their Responses to Climate Change and Human Activities from 1982 to 2020: A Case Study in the Mu Us Sandy Land, China. *Ecol. Indic.* **2022**, *137*, 108745. [[CrossRef](#)]
30. Gu, Z.; Duan, X.; Shi, Y.; Li, Y.; Pan, X. Spatiotemporal Variation in Vegetation Coverage and Its Response to Climatic Factors in the Red River Basin, China. *Ecol. Indic.* **2018**, *93*, 54–64. [[CrossRef](#)]
31. Yang, L.; Guan, Q.; Lin, J.; Tian, J.; Tan, Z.; Li, H. Evolution of NDVI Secular Trends and Responses to Climate Change: A Perspective from Nonlinearity and Nonstationarity Characteristics. *Remote Sens. Environ.* **2021**, *254*, 112247. [[CrossRef](#)]
32. Piao, S.; Liu, Q.; Chen, A.; Janssens, I.A.; Fu, Y.; Dai, J.; Liu, L.; Lian, X.; Shen, M.; Zhu, X. Plant Phenology and Global Climate Change: Current Progresses and Challenges. *Glob. Change Biol.* **2019**, *25*, 1922–1940. [[CrossRef](#)]

33. Li, P.; Wang, J.; Liu, M.; Xue, Z.; Bagherzadeh, A.; Liu, M. Spatio-Temporal Variation Characteristics of NDVI and Its Response to Climate on the Loess Plateau from 1985 to 2015. *Catena* **2021**, *203*, 105331. [CrossRef]
34. Li, Y.; Zheng, Z.; Qin, Y.; Rong, P. Relative Contributions of Natural and Man-Made Factors to Vegetation Cover Change of Environmentally Sensitive and Vulnerable Areas of China. *J. Clean. Prod.* **2021**, *321*, 128917. [CrossRef]
35. Fahad, S.; Hasanuzzaman, M.; Alam, M.; Ullah, H.; Saeed, M.; Khan, I.A.; Adnan, M. *Environment, Climate, Plant and Vegetation Growth*; Springer: Berlin/Heidelberg, Germany, 2020; ISBN 3-030-49732-1.
36. Liu, K.; Li, X.; Wang, S.; Zhang, X. Unrevealing Past and Future Vegetation Restoration on the Loess Plateau and Its Impact on Terrestrial Water Storage. *J. Hydrol.* **2023**, *617*, 129021. [CrossRef]
37. Hoek van Dijke, A.J.; Herold, M.; Mallick, K.; Benedict, I.; Machwitz, M.; Schlerf, M.; Pranindita, A.; Theeuwes, J.J.E.; Bastin, J.-F.; Teuling, A.J. Shifts in Regional Water Availability Due to Global Tree Restoration. *Nat. Geosci.* **2022**, *15*, 363–368. [CrossRef]
38. Zhang, J.; Zhang, Y.; Sun, G.; Song, C.; Dannenberg, M.P.; Li, J.; Liu, N.; Zhang, K.; Zhang, Q.; Hao, L. Vegetation Greening Weakened the Capacity of Water Supply to China's South-to-North Water Diversion Project. *Hydrol. Earth Syst. Sci.* **2021**, *25*, 5623–5640. [CrossRef]
39. Yang, S.; Liu, J.; Wang, C.; Zhang, T.; Dong, X.; Liu, Y. Vegetation Dynamics Influenced by Climate Change and Human Activities in the Hanjiang River Basin, Central China. *Ecol. Indic.* **2022**, *145*, 109586. [CrossRef]
40. Liu, H.; Zheng, L.; Yin, S. Multi-Perspective Analysis of Vegetation Cover Changes and Driving Factors of Long Time Series Based on Climate and Terrain Data in Hanjiang River Basin, China. *Arab. J. Geosci.* **2018**, *11*, 509. [CrossRef]
41. Chen, T.; Xia, J.; Zou, L.; Hong, S. Quantifying the Influences of Natural Factors and Human Activities on NDVI Changes in the Hanjiang River Basin, China. *Remote Sens.* **2020**, *12*, 3780. [CrossRef]
42. Ebrahimi Khusfi, Z.; Khosroshahi, M.; Roustaei, F.; Mirakbari, M. Spatial and Seasonal Variations of Sand-Dust Events and Their Relation to Atmospheric Conditions and Vegetation Cover in Semi-Arid Regions of Central Iran. *Geoderma* **2020**, *365*, 114225. [CrossRef]
43. Li, C.; Jia, X.; Zhu, R.; Mei, X.; Wang, D.; Zhang, X. Seasonal Spatiotemporal Changes in the NDVI and Its Driving Forces in Wuliangsu Lake Basin, Northern China from 1990 to 2020. *Remote Sens.* **2023**, *15*, 2965. [CrossRef]
44. Wang, F.; Ma, Y.; Darvishzadeh, R.; Han, C. Annual and Seasonal Trends of Vegetation Responses and Feedback to Temperature on the Tibetan Plateau since the 1980s. *Remote Sens.* **2023**, *15*, 2475. [CrossRef]
45. Wang, S.; Zhang, Y.; Ju, W.; Porcar-Castell, A.; Ye, S.; Zhang, Z.; Brümmer, C.; Urbaniak, M.; Mammarella, I.; Juszczak, R.; et al. Warmer Spring Alleviated the Impacts of 2018 European Summer Heatwave and Drought on Vegetation Photosynthesis. *Agric. For. Meteorol.* **2020**, *295*, 108195. [CrossRef]
46. Ma, M.; Wang, Q.; Liu, R.; Zhao, Y.; Zhang, D. Effects of Climate Change and Human Activities on Vegetation Coverage Change in Northern China Considering Extreme Climate and Time-Lag and -Accumulation Effects. *Sci. Total Environ.* **2023**, *860*, 160527. [CrossRef] [PubMed]
47. Wu, D.; Zhao, X.; Liang, S.; Zhou, T.; Huang, K.; Tang, B.; Zhao, W. Time-Lag Effects of Global Vegetation Responses to Climate Change. *Glob. Change Biol.* **2015**, *21*, 3520–3531. [CrossRef] [PubMed]
48. Allen, R. An Update for the Calculation of Reference Evapotranspiration. *IcID Bull.* **1994**, *43*, 35–92.
49. Vicente-Serrano, S.M.; Beguería, S.; López-Moreno, J.I. A Multiscalar Drought Index Sensitive to Global Warming: The Standardized Precipitation Evapotranspiration Index. *J. Clim.* **2010**, *23*, 1696–1718. [CrossRef]
50. Hutchinson, M.F.; Xu, T. *Anusplin Version 4.2 User Guide*; Centre for Resource and Environmental Studies, The Australian National University: Canberra, Australia, 2004; p. 54.
51. Sen, P.K. Estimates of the Regression Coefficient Based on Kendall's Tau. *J. Am. Stat. Assoc.* **1968**, *63*, 1379–1389. [CrossRef]
52. Fernandes, R.; Leblanc, S.G. Parametric (Modified Least Squares) and Non-Parametric (Theil–Sen) Linear Regressions for Predicting Biophysical Parameters in the Presence of Measurement Errors. *Remote Sens. Environ.* **2005**, *95*, 303–316. [CrossRef]
53. Chen, J.; Shao, Z.; Huang, X.; Zhuang, Q.; Dang, C.; Cai, B.; Zheng, X.; Ding, Q. Assessing the Impact of Drought-Land Cover Change on Global Vegetation Greenness and Productivity. *Sci. Total Environ.* **2022**, *852*, 158499. [CrossRef]
54. Kendall, M. *Rank Correlation Methods*; Griffin: London, UK, 1975. Available online: https://scholar.google.com/scholar_lookup?title=Rank+Correlation+Methods&author=Kendall,+M.&publication_year=1975 (accessed on 12 October 2022).
55. Xu, J. *Mathematical Methods in Contemporary Geography*; China Higher Education Press: Beijing, China, 2002; p. 224230.
56. Lundberg, S.; Lee, S.-I. A Unified Approach to Interpreting Model Predictions. *Adv. Neural Inf. Process. Syst.* **2017**, *30*, 4768–4777. [CrossRef]
57. Wang, D.; Thunell, S.; Lindberg, U.; Jiang, L.; Trygg, J.; Tysklind, M. Towards Better Process Management in Wastewater Treatment Plants: Process Analytics Based on SHAP Values for Tree-Based Machine Learning Methods. *J. Environ. Manag.* **2022**, *301*, 113941. [CrossRef] [PubMed]
58. Guo, X.; Gui, X.; Xiong, H.; Hu, X.; Li, Y.; Cui, H.; Qiu, Y.; Ma, C. Critical Role of Climate Factors for Groundwater Potential Mapping in Arid Regions: Insights from Random Forest, XGBoost, and LightGBM Algorithms. *J. Hydrol.* **2023**, *621*, 129599. [CrossRef]
59. Jiang, W.; Wang, L.; Zhang, M.; Yao, R.; Chen, X.; Gui, X.; Sun, J.; Cao, Q. Analysis of Drought Events and Their Impacts on Vegetation Productivity Based on the Integrated Surface Drought Index in the Hanjiang River Basin, China. *Atmos. Res.* **2021**, *254*, 105536. [CrossRef]

60. Zhang, T.; Xu, X.; Jiang, H.; Qiao, S.; Guan, M.; Huang, Y.; Gong, R. Widespread Decline in Winds Promoted the Growth of Vegetation. *Sci. Total Environ.* **2022**, *825*, 153682. [[CrossRef](#)]
61. Park, H.; Jeong, S.; Peñuelas, J. Accelerated Rate of Vegetation Green-up Related to Warming at Northern High Latitudes. *Glob. Change Biol.* **2020**, *26*, 6190–6202. [[CrossRef](#)]
62. Islam, A.R.M.T.; Islam, H.M.T.; Shahid, S.; Khatun, M.K.; Ali, M.M.; Rahman, M.S.; Ibrahim, S.M.; Almoajel, A.M. Spatiotemporal Nexus between Vegetation Change and Extreme Climatic Indices and Their Possible Causes of Change. *J. Environ. Manag.* **2021**, *289*, 112505. [[CrossRef](#)]
63. Gan, G.; Liu, Y.; Sun, G. Understanding Interactions among Climate, Water, and Vegetation with the Budyko Framework. *Earth-Sci. Rev.* **2021**, *212*, 103451. [[CrossRef](#)]
64. Xu, X.; Zhang, D.; Zhang, Y.; Yao, S.; Zhang, J. Evaluating the Vegetation Restoration Potential Achievement of Ecological Projects: A Case Study of Yan'an, China. *Land Use Policy* **2020**, *90*, 104293. [[CrossRef](#)]
65. Zhao, A.; Yu, Q.; Feng, L.; Zhang, A.; Pei, T. Evaluating the Cumulative and Time-Lag Effects of Drought on Grassland Vegetation: A Case Study in the Chinese Loess Plateau. *J. Environ. Manag.* **2020**, *261*, 110214. [[CrossRef](#)]
66. Zhou, L.; Zhang, X.; Zhang, Y.; Song, Q.; Myo, S.T.Z.; Zhou, R.; Lin, Y.; Liu, Y.; Bai, K.; Gnanamoorthy, P.; et al. The Cumulative Drought Exert Disruptive Effects on Tropical Rainforests in the Northern Edge of Asia—Based on Decadal Dendrometric Measurements and Eddy Covariance Method. *Agric. For. Meteorol.* **2022**, *316*, 108858. [[CrossRef](#)]

Disclaimer/Publisher's Note: The statements, opinions and data contained in all publications are solely those of the individual author(s) and contributor(s) and not of MDPI and/or the editor(s). MDPI and/or the editor(s) disclaim responsibility for any injury to people or property resulting from any ideas, methods, instructions or products referred to in the content.